Monthly Notices
of the
ROYAL ASTRONOMICAL SOCIETY

MNRAS **435,** 3231–3242 (2013)
Advance Access publication 2013 September 23

doi:10.1093/mnras/stt1519

The WARPS Survey – VIII. Evolution of the galaxy cluster X-ray Luminosity Function

L. A. Koens,[1,2⋆] B. J. Maughan,[2] L. R. Jones,[3] H. Ebeling,[4] D. J. Horner,[5] E. S. Perlman,[6] S. Phillipps[2] and C. A. Scharf[7]

[1]*SUPA, Institute for Astronomy, University of Edinburgh, Royal Observatory, Blackford Hill, Edinburgh EH9 3HJ, UK*
[2]*HH Wills Physics Laboratory, Tyndall Avenue, Bristol BS8 1TL, UK*
[3]*School of Physics and Astronomy, The University of Birmingham, Edgbaston, Birmingham B15 2TT, UK*
[4]*Institute for Astronomy, 2680 Woodlawn Drive, Honolulu, HI 96822, USA*
[5]*NASA Goddard Space Flight Center, Code 660.1, Greenbelt, MD 20771, USA*
[6]*Department of Physics and Space Sciences, Florida Insitute of Technology, 150 West University Boulevard, Melbourne, FL 32901, USA*
[7]*Columbia Astrophysics Laboratory, MC 5247, 550 West 120th St., New York, NY 10027, USA*

Accepted 2013 August 9. Received 2013 August 9; in original form 2012 October 18

ABSTRACT

We present measurements of the galaxy cluster X-ray Luminosity Function (XLF) from the Wide Angle *ROSAT* Pointed Survey (WARPS) and quantify its evolution. WARPS is a serendipitous survey of the central region of *ROSAT* pointed observations and was carried out in two phases (WARPS-I and WARPS-II). The results here are based on a final sample of 124 clusters, complete above a flux limit of 6.5×10^{-14} erg cm^{-2} s^{-1}, with members out to redshift $z \sim 1.05$, and a sky coverage of 70.9 deg^2. We find significant evidence for negative evolution of the XLF, which complements the majority of X-ray cluster surveys. To quantify the suggested evolution, we perform a maximum likelihood analysis and conclude that the evolution is driven by a decreasing number density of high-luminosity clusters with redshift, while the bulk of the cluster population remains nearly unchanged out to redshift $z \approx 1.1$, as expected in a low-density universe. The results are found to be insensitive to a variety of sources of systematic uncertainty that affect the measurement of the XLF and determination of the survey selection function. We perform a Bayesian analysis of the XLF to fully account for uncertainties in the local XLF on the measured evolution, and find that the detected evolution remains significant at the 95 per cent level. We observe a significant excess of clusters in the WARPS at $0.1 < z < 0.3$ and $L_X \approx 2 \times 10^{43}$ erg s^{-1} compared with the reference low-redshift XLF, or our Bayesian fit to the WARPS data. We find that the excess cannot be explained by sample variance, or Eddington bias, and is unlikely to be due to problems with the survey selection function.

Key words: galaxies: clusters: general – cosmology: observations – X-rays: galaxies: clusters.

1 INTRODUCTION

Evolutionary properties of gravitationally bound objects in the Universe are described by models of structure formation. The currently favoured cosmology [flat Λ cold dark matter (ΛCDM)] predicts little change in the abundance of galaxy clusters at late times when the energy density of the Universe becomes dominated by Ω_Λ. The evolution of cluster abundance depends on the growth rate f, which is mainly sensitive to the mean cosmic matter density Ω_m as $f(z) \simeq \Omega_m(z)^\gamma$, where $\gamma \simeq 0.6$ in a universe described by General Relativity (Linder 2005).

Galaxy clusters, the largest objects to have decoupled from the Hubble expansion, are particularly interesting for studying these properties as a result of their X-ray brightness. The X-ray emission is the result of bremsstrahlung emitted by the hot intracluster medium (10^7–10^8 K) which contributes more than 80 per cent of the baryonic content of the cluster. Therefore, the mass of a cluster can be estimated from its luminosity with the use of scaling relations and some simplifying assumptions (Kaiser 1986). The X-ray emitting gas has enabled cluster detections out to high redshift ($z \gtrsim 1$). Hence, X-ray galaxy cluster surveys potentially cover a significant portion of the evolution history of clusters and have high statistical completeness, thus providing the leverage to place tight cosmological constraints (e.g. Borgani et al. 1999; Schuecker et al. 2003; Vikhlinin et al. 2009; Mantz et al. 2010).

⋆ E-mail: lak@roe.ac.uk

© 2013 The Authors
Published by Oxford University Press on behalf of the Royal Astronomical Society

Downloaded from http://mnras.oxfordjournals.org/ at NASA Goddard Space Flight Ctr on September 2, 2014

Early predictions of evolution in the number density of clusters, e.g. Kaiser (1986), pointed towards strong positive evolution – an increase in the number density of clusters with redshift. This prediction assumes a matter power spectrum with a power-law form, and that the heating of gas is solely by adiabatic compression during the collapse of dark matter haloes. The first opportunity to test these predictions came with the Einstein Medium Sensitivity Survey (EMSS; Gioia et al. 1990b), which detected clusters out to $z \approx 0.8$. Contrary to the theoretical prediction, the first teams to test for evolution in the X-ray Luminosity Function(XLF) found strong negative evolution (Gioia et al. 1990a; Edge et al. 1990; Henry et al. 1992). These controversial findings heated the debate and together with the launch of the *ROSAT* X-ray observatory gave rise to a flurry of attempts to measure evolution in the XLF, with some later analyses raising concerns over the Einstein results (e.g. Ellis & Jones 2002).

ROSAT performed an all-sky survey which was used to construct large flux limited cluster samples, from which the local cluster XLF was accurately determined. There are three such surveys: the Brightest Cluster Sample (Ebeling et al. 1998, 2000), the *ROSAT* All-Sky Survey 1 Brightest Sample (de Grandi et al. 1999) and the *ROSAT*-ESO Flux-Limited X-ray (REFLEX) galaxy cluster survey (Böhringer et al. 2001). These local XLFs act as the crucial baseline for quantifying evolution in deeper surveys.

Once the *ROSAT* all-sky survey was completed the observatory remained available for pointed observations, which has resulted in an extensive archive of deep observations, providing the ingredients for many serendipitous X-ray cluster surveys. This includes the Wide Angle *ROSAT* Pointed Survey (Scharf et al. 1997; Perlman et al. 2002; Horner et al. 2008), the subject of this paper. Similar surveys that probe the X-ray Universe out to high redshift include the *ROSAT* International X-ray/Optical Survey (RIXOS; Castander et al. 1995; Mason et al. 2000), the *ROSAT* Deep Cluster Survey (RDCS; Rosati et al. 1995, 1998), the Bright Serendipitous High-Redshift Archival *ROSAT* Cluster (BSHARC) Survey (Romer et al. 2000), the Massive Cluster Survey (MACS) (Ebeling, Edge & Henry 2001), the Brera Multi-scale Wavelet *ROSAT* HRI (BMW-HRI) survey (Moretti et al. 2001; Panzera et al. 2003) *ROSAT* North Ecliptic Pole (NEP) Survey (Henry et al. 2001; Gioia et al. 2001), SSHARC (Burke et al. 2003), and the 160 Square Degree (160SD; Vikhlinin et al. 1998; Mullis et al. 2003, 2004), extended to the 400 Square Degree (400SD) survey (Burenin et al. 2007).

XMM–Newton archival data are also used for surveys based on serendipitous cluster detections. Currently in progress are the XMM Cluster Survey (XCS; Mehrtens et al. 2011), the *XMM–Newton* Distant Cluster Project (XDCP; Fassbender et al. 2011) and the *XMM–Newton* eXtra eXtra Large (XXL) Survey (Pierre et al. 2011). One serendipitous galaxy cluster survey is based on *Chandra* archival data and is part of the *Chandra* Multiwavelength Project (CHaMP; Barkhouse et al. 2006).

The most recent determination of the XLF was performed by Mullis et al. (2004) using 201 clusters from the 160SD catalogue. This work found significant evidence for negative evolution of the XLF at the bright end. That is, the number density of high-luminosity clusters was lower at $0.6 < z < 0.8$ than in the local Universe. Meanwhile Mantz et al. (2008) used the XLF of several *ROSAT* cluster surveys at $z < 0.5$ to measure the cluster mass function and hence constrain cosmological parameters.

In this paper we investigate the evolution of the XLF of a sample of 124 Wide Angle *ROSAT* Pointed Survey (WARPS) galaxy clusters detected above a flux limit of 6.5×10^{-14} erg cm^{-2} s^{-1} over a total area of 70.9 deg^2, and covering a wide redshift range ($0.02 < z < 1.10$). The survey design was outlined in Scharf et al. (1997) and the catalogues are presented in two separate papers: WARPS-I (Perlman et al. 2002) and WARPS-II (Horner et al. 2008). The evolution of the WARPS galaxy clusters has previously been investigated using phase-I of the survey. Jones et al. (1998) found no significant evolution in the $\log N - \log S$ relation from the WARPS-I sample and a preliminary measurement of the XLF (constructed when the survey was complete for $z < 0.85$) was also found to be consistent with no evolution (Jones et al. 2000).

This work represents a useful cross-check and extension of the Mullis et al. (2004) results. While the WARPS survey covers a smaller area, it is deeper; the 160SD XLF extends to $z \approx 0.7$. Importantly, while both surveys are drawn from *ROSAT* pointed observations, the cluster detection and confirmation strategies differ significantly, allowing us to assess the sensitivity of the evolution results to those factors.

The current paper is organized as follows. Section 2 briefly reviews the WARPS survey and the combined WARPS-I + WARPS-II sample. The selection function of the full survey is presented for the first time. In Section 3 the XLF is presented for different redshift ranges. Subsequently, in Section 4 a maximum likelihood (ML) analysis robustly assesses evolution in the XLF. In Sections 5 and 6 we discuss our results and summarize our conclusions. Throughout the paper errors are quoted at the 68 per cent confidence level and a ΛCDM cosmology of $H_0 = 70\,h_{70}$ km s^{-1} Mpc^{-1}, $\Omega_{\rm m} = 0.3$ and $\Omega_\Lambda = 0.7$ is adopted. All fluxes are corrected for absorption, and are quoted in the observer's frame 0.5–2 keV band. Luminosities are converted to the rest frame 0.5–2 keV band of each cluster.

2 THE WARPS CLUSTER SAMPLE

The survey is based entirely on serendipitous detections in *ROSAT* images from pointed observations with the Position Sensitive Proportional Counter (PSPC) instrument. Here we summarize the key facts and direct the reader to Scharf et al. (1997) for full details of the survey methodology.

PSPC fields were selected based on the following criteria. The fields are at a Galactic latitude of $|b| \geq 20^\circ$, have exposure times of $t_{\rm exp} \geq 8$ ks, are non-overlapping and the original target is not a galaxy cluster or some other source such as a bright star that would hamper optical follow-up. Out of the ∼7000 fields in the High Energy Astrophysics Science Archive Research Center archive 381 satisfy the criteria.

Sources were detected with Voronoi Tessellation and Percolation (VTP) (Ebeling & Wiedenmann 1993) in an annulus of inner radius 3 arcmin and outer radius 15 arcmin. VTP does not discriminate against shape or size and is particularly sensitive to sources of low surface brightness. WARPS has assessed the efficacy of VTP as a source detection algorithm by optically imaging all X-ray candidates in WARPS-I lacking counterparts on existing sky survey plates.

The completeness and efficiency of the VTP detection algorithm were established with simulations of azimuthally symmetrical clusters, inserted into PSPC fields. The detected flux is extrapolated to infinite radius assuming a β profile. Although *Chandra* and *XMM–Newton* data have revealed significant substructure in cluster images up to $z \sim 1$, the relatively poor PSPC angular resolution means that the assumption of spherical symmetry is not expected to strongly affect the detection efficiency and flux estimation. This conclusion is supported by the good agreement between the WARPS and other *ROSAT* serendipitous surveys that used independent detection algorithms and selection functions (Horner et al. 2008, this work). Based on our simulations a statistically complete sample

Downloaded from http://mnras.oxfordjournals.org/ at NASA Goddard Space Flight Ctr on September 2, 2014

was defined, comprising 124 clusters above a conservative flux of 6.5×10^{-14} erg cm^{-2} s^{-1} (Horner et al. 2008) (145 sources were confirmed by WARPS).

For clusters in common, WARPS fluxes were found to be in reasonable agreement with those determined by other serendipitous *ROSAT* surveys (Horner et al. 2008). Spectroscopic redshifts were obtained for all clusters, with 2 or more concordant redshifts required to confirm a cluster. WARPS did not obtain near-infrared imaging of cluster candidates, placing an upper limit on the redshift out to which clusters can be detected. This limit is ∼1.1, and the uncertainty arising from this is addressed in Section 4.1.1.

In combining WARPS-I and WARPS-II catalogues, it was found that background levels were missing for one WARPS-I field and 27 WARPS-II fields. The background level of each field is required in order to compute the selection function, and so these were remeasured from the archived PSPC data. The *ROSAT* PSPC data have been reprocessed since the cluster detection was performed, so we checked the background measurements for all WARPS-I fields using the currently available PSPC data against our original measurements. The new measurements were found to be ∼7 per cent lower on average, depending somewhat on the source detection algorithm used to exclude sources in each field. We thus renormalized the background measurements for the 28 missing fields in the combined WARPS catalogue by this factor, for consistency with the data used for cluster detection. We investigated the impact of this systematic effect on the selection function, and found it to be insensitive to whether or not this background scaling was applied to the 28 missing fields. This is not surprising given the small magnitude of the correction and the small fraction of fields affected.

In Fig. 1 the WARPS clusters are plotted in the luminosity-redshift plane. The fluxes of the clusters have been *K*-corrected to the cluster rest frame assuming an Astrophysical Plasma Emission Code thermal plasma model (Smith et al. 2001), for which we set the metallicity to 0.3 $Z_\odot$. The plasma temperature required for this conversion was estimated iteratively from the X-ray luminosity using the luminosity temperature scaling relation of Markevitch (1998), although the magnitude of the *K*-correction was insensitive to this choice.

The selection function for WARPS-I and WARPS-II combined is shown in Fig. 2 and is based on 381 PSPC fields. The effective sky

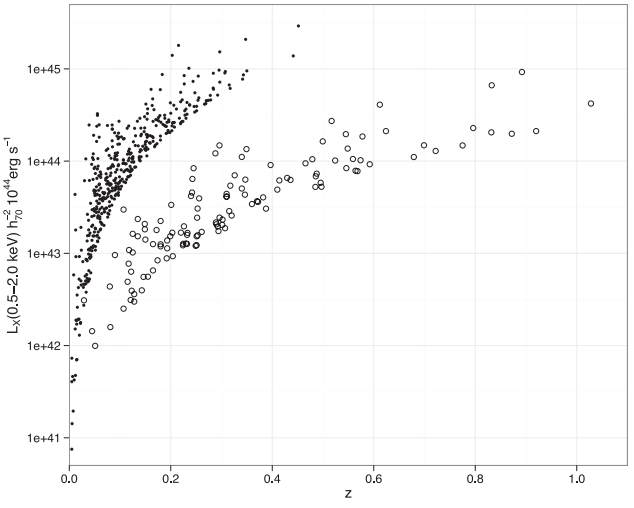

Figure 1. The WARPS clusters (hollow points) as points in the L_X–z plane. Also plotted is the REFLEX sample (solid points), which provides the low-redshift reference XLF for this study (Böhringer et al. 2001).

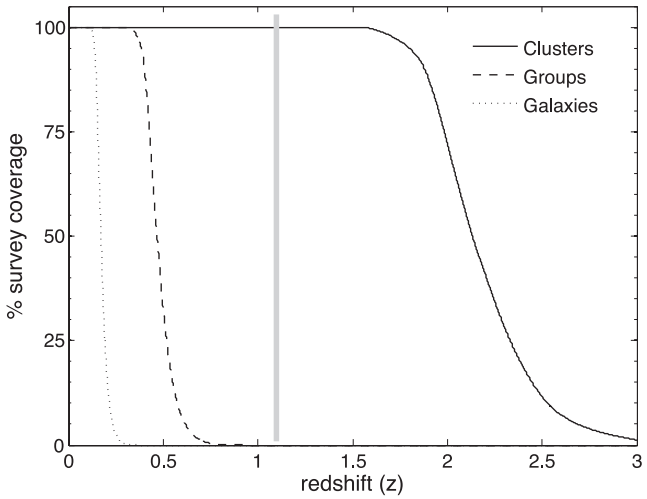

Figure 2. Survey coverage for three classes of objects as a function of redshift. The objects are defined as: elliptical galaxies with $L_X(0.5-2.0\,\mathrm{keV}) = 1 \times 10^{42}\,\mathrm{erg\,s^{-1}}$ and effective core radius $r_c = 50$ kpc, groups with $L_X(0.5-2.0\,\mathrm{keV}) = 1 \times 10^{43}\,\mathrm{erg\,s^{-1}}$ and effective core radius $r_c = 100$ kpc, and clusters with $L_X(0.5-2.0\,\mathrm{keV}) = 5 \times 10^{44}\,\mathrm{erg\,s^{-1}}$ and effective core radius $r_c = 250$ kpc. The grey line represents the approximate upper redshift limit imposed by the lack of near infra-red follow-up of cluster candidates.

coverage for an object of given luminosity and extent is determined by the performance of VTP, the degrading point spread function PSF with off-axis angle, and the background levels and exposure times of the fields. The variance in the field properties of the survey alters the steepness of the decrease; e.g. if all the fields were the same, we expect a much more sudden drop from 100 to 0 per cent. We find the curve for the full survey to be very similar to that for WARPS-I [fig. 9 in Scharf et al. (1997)].

3 THE X-RAY LUMINOSITY FUNCTION

The XLF, conventionally given the symbol ϕ, is the comoving number density n of objects per luminosity interval:

$$\phi(L_X, z) = \frac{\mathrm{d}n(L_X, z)}{\mathrm{d}L_X}. \quad (1)$$

The Schechter function (Schechter 1976) is the canonical, parametric representation of the luminosity function:

$$\phi(L_X, z)\mathrm{d}L_X = \phi^* \left(\frac{L_X}{L_X^*}\right)^{-\alpha} \exp\left(-\frac{L_X}{L_X^*}\right)\left(\frac{\mathrm{d}L_X}{L_X^*}\right), \quad (2)$$

where the parameter ϕ^* normalizes the XLF, and α determines the steepness at $L_X < L_X^*$.

The conventional method to compute the differential XLF is the $1/V_{max}$ method (Schmidt 1968; Avni & Bahcall 1980), where V_{max} denotes the maximum comoving volume, given by

$$V_{max} = \int_{z_{min}}^{z_{max}} \Omega(f_X, r_\theta)\frac{\mathrm{d}V(z)}{\mathrm{d}z}\mathrm{d}z, \quad (3)$$

where $\Omega(f_X, r_\theta)$ is the sky coverage as a function of flux $f_X(L_X, z)$ and angular extent $r_\theta(r_c, z)$ (here r_c is the core radius of the cluster surface brightness distribution, conventionally parametrized with a β-model), and $\mathrm{d}V(z)/\mathrm{d}z$ is the differential, comoving volume, which is strongly sensitive to the cosmological framework. The maximum comoving volume is calculated for all N galaxy clusters. The XLF is

Downloaded from http://mnras.oxfordjournals.org/ at NASA Goddard Space Flight Ctr on September 2, 2014

then obtained by summing the corresponding density contributions per luminosity bin, that is

$$\phi(L_{X_j}, z) = \frac{1}{\Delta L_{X_j}} \sum_{i=0}^{N_j} \frac{1}{V_{\max,i}}, \quad (4)$$

where the subscript j denotes the jth bin. Due to the sensitivity to the choice of binning, the method is less ideal for quantifying evolution. However, it is a conventional way of presenting a sample of objects, so we include it here to allow easy comparisons with previous work.

Alternatively, Page & Carrera (2000) provide an estimate of ϕ, which expression is obtained by integrating (1) and noting that ϕ changes little compared to the survey volume element in the volume–luminosity plane, such that it can be taken out of the integral, giving

$$\phi(L_{X_j}, z) = \frac{N_j}{\int_{L_{X,\min}}^{L_{X,\max}} \int_{z_{\min}}^{z_{\max}} \Omega(f_X, r_\theta) \frac{dV(z)}{dz} dz dL_X}, \quad (5)$$

where L_{X_j} is the bin centre and N_j is the number of clusters in the jth bin.

We apply the method of Page & Carrera (2000) to account for the flux limit of the survey to effectively decrease the width of some of the bins, enhancing the XLF. The Page–Carrera estimator was also deployed by Mullis et al. (2004), who found a marginal increase at the faint end of the XLF compared to the $V_{\max}$ estimator. Our results were similarly insensitive to the choice of volume estimator; the uncertainties at the faint end of the XLF are dominated by those arising from small number statistics, the statistical error on f_X and the uncertainty on r_θ.

3.1 The WARPS XLF

In order to present the binned WARPS XLF, we divide the clusters according to their redshifts to study the local ($0.02 < z < 0.3$; 67 clusters), intermediate-redshift ($0.3 < z < 0.6$; 44 clusters), and high-redshift ($0.6 < z < 1.1$; 13 clusters) populations, similar to Mullis et al. (2004).

We apply the same L_X binning as Mullis et al. (2004) to allow for comparison. Poisson errors on the counts in each luminosity bin are provided by Gehrels (1986), which are much larger than the flux measurement errors.

Good knowledge of the local XLF is essential for studying its evolution and is provided with great accuracy by the *ROSAT* all-sky survey. The XLF of the local WARPS sample of 67 $0.02 < z < 0.3$ clusters is shown in Fig. 3. The lower redshift limit is set to $z = 0.02$ below which many clusters become too extended relative to the size of the PSPC fields to be detected. Over this redshift range the WARPS XLF agrees remarkably well with the all-sky samples, represented by the REFLEX model in Fig. 3.

There appears to be a high number density of clusters at $L_{X(0.5\text{–}2.0\,\mathrm{keV})} \approx 1.5 \times 10^{43}\,\mathrm{erg\,s^{-1}}$ compared to the Schechter function. We note that this feature is also present in the local XLF of the 160SD sample (Mullis et al. 2004, fig. 4) We test the significance of this excess in Section 3.2, and discuss possible interpretations in Section 4.2.

In Fig. 4 we show the intermediate- and high-redshift XLFs along with the local REFLEX Schechter function. The majority of data points of both the intermediate- and high-redshift XLF are slightly low compared to the local baseline. This is a first indication from the data of negative evolution. Whether this is significant will be addressed in the next section.

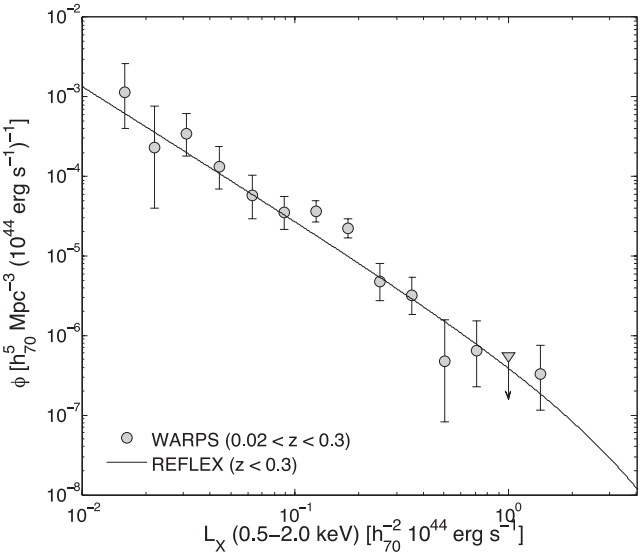

Figure 3. The XLF from the local WARPS sample along with the best-fitting Schechter function of the REFLEX sample.

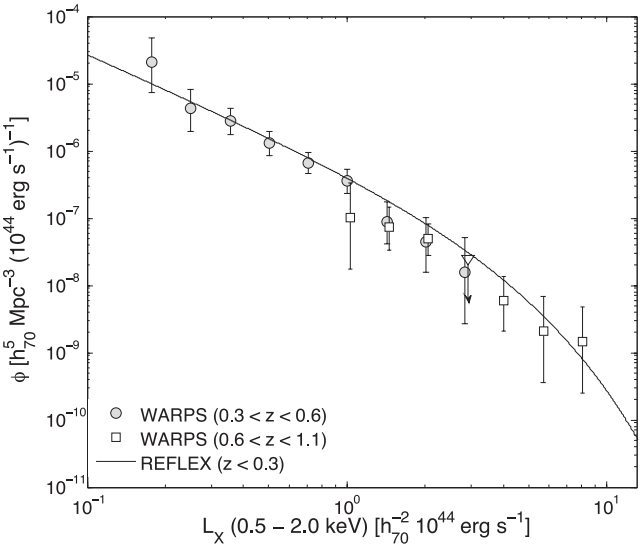

Figure 4. The XLF from the intermediate- and high-redshift WARPS samples along with the best-fitting Schechter function of the REFLEX sample.

3.2 Expected versus observed numbers

The expected number of objects in the luminosity-redshift plane is obtained by integrating equation (1)

$$N_{\exp} = \int_{L_{X,\min}}^{L_{X,\max}} \int_{z_{\min}}^{z_{\max}} \phi(L_X, z) \Omega(f_X, r_\theta) \frac{dV(z)}{dz} dz dL_X. \quad (6)$$

As mentioned in Section 3 the XLF changes little compared to the volume element. Hence we can predict the number of clusters for any of the WARPS subsets based on the local reference XLF ϕ_{local}, the observed XLF for the subset ϕ_{observed}, and the number of clusters observed in that subset N_{observed}:

$$N_{\exp} \approx N_{\mathrm{observed}} \times \frac{\phi_{\mathrm{local}}}{\phi_{\mathrm{observed}}}. \quad (7)$$

Downloaded from http://mnras.oxfordjournals.org/ at NASA Goddard Space Flight Ctr on September 2, 2014

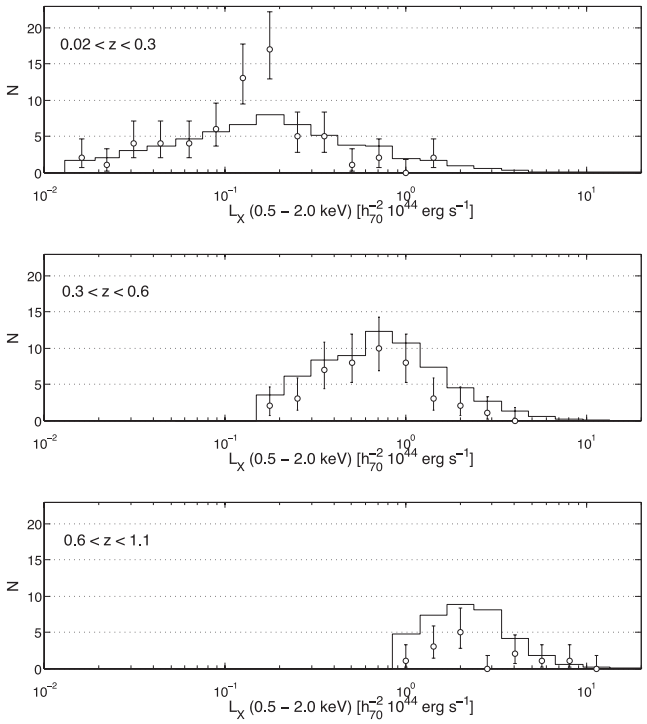

Figure 5. Expected cluster numbers (solid line) versus observed (dots) per luminosity bin for the local, intermediate- and high-redshift samples. The expected number of clusters is calculated per luminosity bin from equation (6).

If the local reference XLF is a good description of the WARPS XLF, and there is no evolution, then $N_{\rm exp}$ should be consistent with $N_{\rm observed}$ for all subsets.

Using the REFLEX best-fitting Schechter function as the local reference, we compute the expected cluster numbers for each luminosity bin in each of the WARPS subsets. The results are plotted in Fig. 5. When integrated over the full range of luminosities, 60 clusters are expected from equation (7) for the low-z subset, instead of the 67 observed. For the intermediate-z subset, 67 are predicted instead of the 44 observed, and for the high-redshift subset, the local relation predicts 36 clusters instead of the 13 that are observed. The differences for the low- and intermediate-redshift subsets are not strongly significant, but the lack of high-z clusters compared to the local prediction is significant at $>4\sigma$, assuming Poisson errors on both numbers.

Fig. 5 also illustrates the excess of clusters around $L_{\rm X(0.5–2.0\,keV)} \approx 1.5 \times 10^{43}$ erg s^{-1} in the low-z subset seen in Fig. 3. Over the two bins with excess counts, there are 28 clusters observed, while only 14 are predicted by the REFLEX XLF. This is a significant excess; the probability of observing $N > 27$ for a Poisson distribution with a mean of 14 is 6.4×10^{-4}. The same analysis was also applied to the larger low-z subset of the 160SD sample. According to equation (7), the number of clusters predicted by the local REFLEX XLF over the two bins with excess counts for the 160SD sample is 18, significantly lower than the observed number of 40 clusters [$P(N > 39) = 5.3 \times 10^{-6}$ for a Poisson distribution with mean 18].

The number of clusters, $N_{\rm mod}$, predicted by the REFLEX fit is uncertain due to the errors on the REFLEX Schechter function parameters. Assuming that the covariance in the REFLEX Schechter function parameters is similar to that found in our fit (section 4.1.3), then the resulting uncertainty on the REFLEX $N_{\rm mod}$ is estimated to be 26 per cent. As the observed number counts are a Poissonian realization of the model prediction, the probability of observing $\geqslant N_{\rm obs}$ clusters for a set of model parameters θ which predicts a number $N_{\rm mod}$ is

$$P(N_{\rm obs}|\theta) = \int P(\geqslant N_{\rm obs}|N_{\rm mod})P(N_{\rm mod}|\theta){\rm d}N_{\rm mod}. \quad (8)$$

We model the first probability distribution as a Poisson distribution and the second as a Gaussian with mean 14 and standard deviation 3.7, which results in a probability of observing at least 28 clusters in this luminosity bump of 1 per cent. The corresponding probability for the bump in the 160SD sample is 0.1 per cent.

3.3 Evolving Schechter function

Here we deploy the ML analysis first set out by Marshall et al. (1983), which fits an evolving Schechter function to the distribution of objects in luminosity redshift space. The treatment is free from arbitrary binning and with the generalization of Mullis et al. (2004) accounts for flux uncertainties. We briefly summarize the method and apply it to the WARPS sample.

The XLF is characterized as an evolving Schechter function

$$\phi(L_{\rm X}, z){\rm d}L_{\rm X} = \phi^*(z)\left[\frac{L_{\rm X}}{L^*_{\rm X}(z)}\right]^{-\alpha} \exp\left[-\frac{L_{\rm X}}{L^*_{\rm X}(z)}\right]\left[\frac{{\rm d}L_{\rm X}}{L^*_{\rm X}(z)}\right]. \quad (9)$$

The parameters, except for α, are allowed to evolve as follows:

$$\phi^*(z) = \phi^*_0\left[\frac{1+z}{1+z_0(L_{\rm X})}\right]^A, \quad (10)$$

$$L^*_{\rm X}(z) = L^*_{\rm X,0}\left[\frac{1+z}{1+z_0(L_{\rm X})}\right]^B, \quad (11)$$

where ϕ^*_0 and $L^*_{\rm X,0}$ are adopted from the local XLF. Due to the flux limit of the surveys, the median redshift z_0 increases with luminosity bin and is given by the local XLF. A deviation from $A = B = 0$ indicates evolution.

To be free from arbitrary binning, the luminosity redshift grid is chosen to be sufficiently fine for there to be either 1 or 0 clusters in each cell. We achieve this with ${\rm d}z = 0.01$ and ${\rm d}L_{\rm X} = 0.1 \times 10^{43} h^{-2}$ erg s^{-1} for the WARPS sample. In each cell the expected number of clusters is calculated

$$\lambda(L_{\rm X}, z){\rm d}L_{\rm X}{\rm d}z = \phi(L_{\rm X}, z)\Omega(f_{\rm X}, r_\theta)\frac{{\rm d}V(z)}{{\rm d}z}{\rm d}L_{\rm X}{\rm d}z. \quad (12)$$

The likelihood function $\mathcal{L}$ describes the joint probability of detecting 1 cluster at each occupied cell i and 0 in each empty cell j and is given by

$$\mathcal{L} = \prod_i \lambda(L_{\rm X,i}, z_i){\rm d}L_{\rm X}{\rm d}z\, \exp\left[-\lambda(L_{\rm X,i}, z_i){\rm d}L_{\rm X}{\rm d}z\right] \times \prod_j \exp\left[-\lambda(L_{\rm X,i}, z_i){\rm d}L_{\rm X}{\rm d}z\right], \quad (13)$$

which makes use of the Poisson distribution and is valid when the number of expected clusters $\ll 1$ as expected for small cells. To account for the uncertainties on the measured fluxes, we smooth the objects by a Gaussian in the luminosity direction, in the same way as in Mullis et al. (2004). The amount of smoothing is based on the 1σ flux errors. Redshift errors are not taken into account, since they are typically much smaller.

We calculate $\Delta S = S(A, B) - S(A_{\rm best}, B_{\rm best})$, where $S = -2\ln\mathcal{L}$. In Fig. 6 we plot contours of $\Delta S = 2.30$, 6.17 and 11.8, which correspond to the 1σ, 2σ and 3σ confidence limits.

Downloaded from http://mnras.oxfordjournals.org/ at NASA Goddard Space Flight Ctr on September 2, 2014

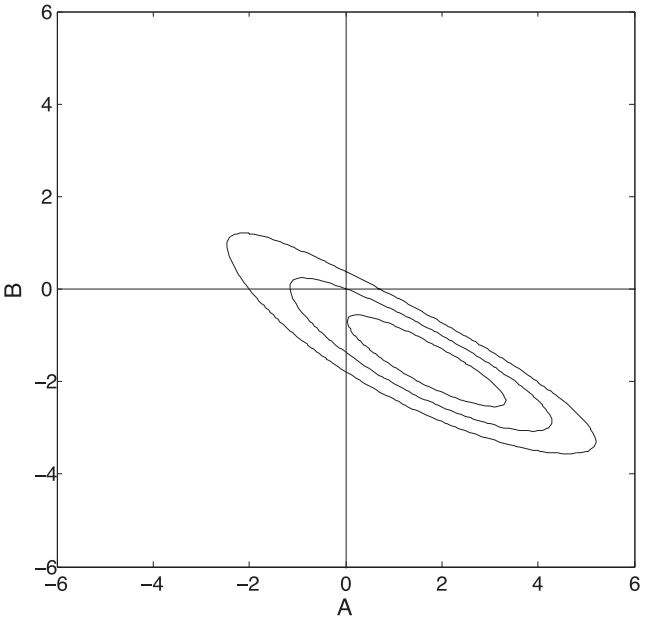

Figure 6. Likelihood contours for the evolution parameters A and B, defined in equations (10) and (11), based on a comparison of the local REFLEX Schechter function and the complete WARPS distribution of clusters in luminosity redshift space. Contours show the 1σ, 2σ and 3σ confidence limits.

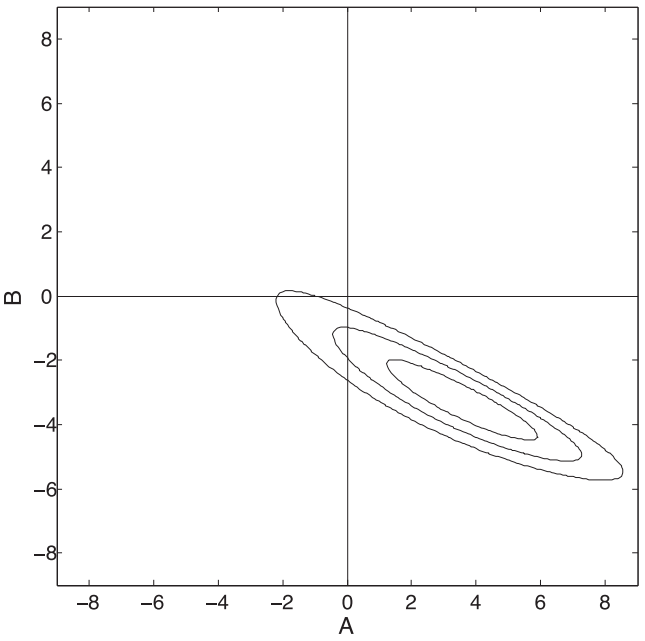

Figure 7. Likelihood contours for the evolution parameters A and B, defined in equations (10) and (11), based on a comparison of the local REFLEX Schechter function and the $z > 0.3$ WARPS clusters. Contours show the 1σ, 2σ and 3σ confidence limits.

The contours for WARPS are shown in Fig. 6, with evolution measured relative to the local XLF from REFLEX, for which we used all 124 WARPS clusters. We find evidence for negative evolution that is significant at 2σ, with $A = -1.88 \pm 0.62$ and $B = -1.76 \pm 0.53$. Stronger evidence for evolution was measured using only the WARPS clusters at $z > 0.3$. The same methodology was applied, and the resulting confidence contours on A and B are shown in Fig. 7. The best-fitting parameters for both samples are given in Table 1.

4 DISCUSSION

4.1 Evolution in the XLF

The comparison of expected and observed cluster number counts, and the ML analysis of the unbinned cluster population both strongly support negative evolution of the XLF. The evolution in ϕ^* and $L_{\rm X}^*$ is degenerate, as is apparent in Fig. 6, but the net effect is significant, and consistent with a decrease in the number density of massive, high-luminosity clusters with redshift, as expected in a ΛCDM hierarchical universe. This is illustrated in Fig. 8, which shows the best-fitting evolution of the REFLEX $z = 0$ Schechter function.

In the ML analysis of Section 3.3 we assume no evolution in the parameter α. Here we test whether this is justified by calculating ΔS for the parameter C defined as

$$\alpha(z) = \alpha_0 \left[\frac{1+z}{1+z_0(L_{\rm X})}\right]^C \qquad (14)$$

and use our best-fitting parameters A and B from Section 3.3. We find $C_{\rm best} = 0.05 \pm 0.17$, and for $A = B = 0$ we have $C_{\rm best} = -0.05 \pm 0.17$. This is reassuring, since in the hierarchical picture of structure formation we expect evolution to occur at the bright end, whereas α determines the slope at fainter luminosities.

The negative evolution measured in the WARPS XLF is in very good agreement with that found for the 160SD (particularly for the $z > 0.3$ subset), and agrees qualitatively with previous measurements of negative evolution in the XLF (see fig. 8 in Mullis et al. 2004). We note that the 160SD evolution was measured with respect to the BCS XLF, whereas we used the REFLEX XLF for our low-redshift baseline, so the agreement in evolution measures suggests that the choice of baseline does not strongly affect the measured evolution. The uncertainty on the local XLF and other systematics affecting the evolution measurements are discussed below.

4.1.1 Uncertainty on $z_{\rm max}$

The upper redshift limit $z_{\rm max}$ for the high-redshift sample is uncertain due to the lack of near infra-red follow-up of cluster candidates. To our knowledge it is the first time this issue has been considered in the determination of the cluster XLF. The RDCS survey included near infra-red imaging which resulted in the successful detection of four clusters beyond redshift 1. However, these fall below the flux limit of their statistically complete sample, which has $z_{\rm max} = 0.83$. The detection and optical confirmation in WARPS of a cluster at $z = 1.028$ is consistent with our estimate of $z_{\rm max} \approx 1.1$, but the exact limit will depend on the characteristics of the galaxy populations and the photometric limits of the optical imaging for each cluster, so is not well defined.

As can be seen in Fig. 2, for very luminous clusters the sky coverage of 100 per cent is maintained well beyond the limit set by the optical observations. This means that the product $\Omega(f_{\rm X}, r_\theta) \times \frac{{\rm d}V(z)}{{\rm d}z}$ is non-zero in equation (5). Hence, an increase in $z_{\rm max}$ suppresses the XLF in those bins that represent sufficiently high X-ray luminosities. Although the influence of the choice of $z_{\rm max}$ on the XLF is suppressed by the flux limit, a too high value for $z_{\rm max}$ could falsely suggest negative evolution, whereas a too low value boosts the bright end towards the opposite conclusion.

Downloaded from http://mnras.oxfordjournals.org/ at NASA Goddard Space Flight Ctr on September 2, 2014

Table 1. Best-fitting XLF parameters. The REFLEX parameters are taken from Böhringer et al. (2002), for a ΛCDM cosmology. The ML fits assumed XLF shape parameters fixed at the REFLEX best-fitting values. The Bayesian fit used the REFLEX values as priors, as discussed in Section 4.1.3.

Data set	Redshift	ϕ^* $10^{-7}\,h_{70}^3\,\mathrm{Mpc}^{-3}$	α	L_X^* $10^{44}\,h_{70}^{-2}$	A	B
REFLEX	$z < 0.3$	2.94 ± 0.82	1.690 ± 0.045	2.64 ± 0.29	–	–
WARPS ML	$z > 0.02$	2.94	1.690	2.64	1.88 ± 0.62	-1.76 ± 0.53
WARPS ML	$z > 0.3$	2.94	1.690	2.64	3.60 ± 0.95	-3.37 ± 0.56
WARPS Bayesian	$z > 0.02$	3.68 ± 0.87	1.79 ± 0.04	2.59 ± 0.35	-0.09 ± 1.19	-0.93 ± 0.58

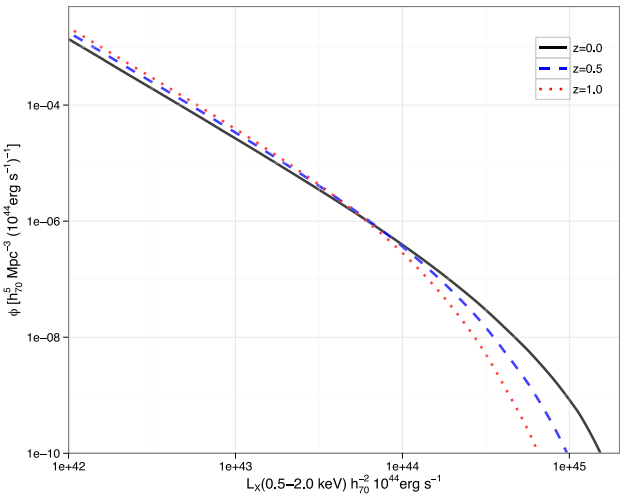

Figure 8. Schechter functions with best-fitting evolution parameters from the ML analysis to the full sample. The lines show the form of the Schechter function at redshifts 0, 0.5 and 1.

We tested the robustness of the evolution measurement to $z_{\max}$ by reducing $z_{\max}$ to $z = 1$ and excluding the $z = 1.028$ cluster from the analysis. The contours in the $A - B$ plane were changed negligibly. This is a conservative approach, and shows our measured evolution is insensitive to the choice of $z_{\max}$. If the effective $z_{\max}$ of the survey is actually larger than the assumed $z = 1.1$, then our non-detection of clusters beyond $z = 1.03$ would imply stronger evolution than that measured here.

4.1.2 *Cluster surface brightness*

Although we refer to the statistically complete WARPS sample as 'flux-limited', in practice it is the X-ray surface brightness and not the flux that determines whether or not a cluster is detected. To a first approximation, the surface brightness is related to the cluster flux by the core radius r_c, that sets the spatial scale of the surface brightness distribution. This then enters the XLF through the computation of the detection volumes of the clusters. Given the relatively large PSF of the PSPC at the off-axis angles considered in WARPS, we do not expect our results to be sensitive to the choice of core radius, with the strongest effects expected at the faint end of the local XLF, which is most sensitive to uncertainties in the selection function.

For each WARPS cluster, a core radius was estimated from the PSPC data as the radius at which the surface brightness, fitted by a β-model with $\beta = 2/3$, is a factor of $2^{1/\beta}$ lower than the central value. The uncertainties on the individual core radii are large, but the average r_c for WARPS is ∼100 kpc, whereas *Chandra* observations of clusters show an average core radius of ∼150 kpc (Maughan et al. 2008).

A disadvantage of the Page-Carrera technique is that information about the core radius of the individual clusters is difficult to include. Thus when applying this technique, a fixed core radius of 102 kpc (average WARPS) was assumed for each cluster. However, using the $V_{\max}$ technique it was possible to investigate the effect of varying r_c. We found that the $V_{\max}$ technique yields nearly identical XLFs for a uniform core radius of 100 kpc (average WARPS), 150 kpc (average *Chandra*) and the individual core radii measured from the PSPC data.

4.1.3 *Uncertainties on the local XLF*

In order to assess the impact of uncertainties on the form of the low-redshift XLF on the measured evolution, we adopted a Bayesian approach to fitting the XLF. The posterior probability distribution for the set of model parameters $\Theta = (\phi^*, L_X^*, \alpha, A, B)$ given the observed data $\boldsymbol{D}$ (the luminosity and redshift of each cluster) is given in the normal way by

$$P(\Theta|\boldsymbol{D}) \propto P(\boldsymbol{D}|\Theta)P(\Theta). \quad (15)$$

Here the first term on the right is the likelihood function, and the second term is the prior probability distribution of the model parameters. This approach allows us to adopt the REFLEX low-z XLF parameters and their uncertainties as priors on ϕ^*, L_X^*, α, which can then be marginalized over. We adopt weak priors on A and B, simply assigning each a Gaussian distribution with mean zero, and standard deviation 100. We also generalize the likelihood expression from equation (13) to include the statistical scatter of the measured luminosities. This accounts for the possibility that clusters that are nominally below the flux limit may be observed to be above the flux limit due to our noisy measurement of L_X (this is a source of Eddington bias and is discussed further below.).

We divide the L_X,z parameter space into cells i, j with coordinates $(L_{X,i}, z_j)$ and widths $(dL_{X,i}, dz_j)$. As before, the XLF model predicts a number of clusters in cell i, j as

$$N_{\mathrm{mod},ij} = \lambda(L_{X,i}, z_j, \Theta)\mathrm{d}L_{X,i}\mathrm{d}z_j. \quad (16)$$

However, the final number of clusters expected in cell i, j includes contributions from all of the other cells in the L_X direction, due to the noisy measurement of L_X. The contribution from a cell at $L_{X,k}$, z_j to the number counts in a cell at $L_{X,i}$, z_j is

$$N_{\mathrm{exp},ijk} = N_{\mathrm{mod},ik}P(L_{X,j}|L_{X,k}, \sigma_k)dL_{X,j}. \quad (17)$$

The probability term here models the measurement noise on a cluster with 'true' luminosity $L_{X,k}$ as a Gaussian with a mean $L_{X,k}$ and standard deviation σ_k. We model the increasing precision of the luminosity measurement with cluster flux by setting σ_k to be inversely proportional to the square root of the flux at $L_{X,k}$, z_j, as expected for measurements dominated by counting statistics. The constant

Downloaded from http://mnras.oxfordjournals.org/ at NASA Goddard Space Flight Ctr on September 2, 2014

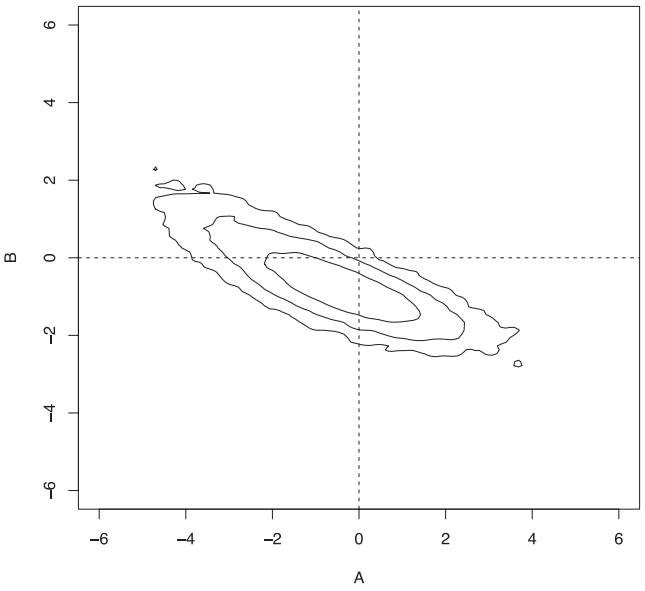

Figure 9. Likelihood contours for the evolution parameters A and B, defined in equations (10) and (11), based on a Bayesian analysis and marginalizing over the uncertainty on the shape parameters of the local XLF. Light grey contours show the constraints from the ML analysis. Contours show the 1σ, 2σ and 3σ confidence limits.

of proportionality is set to give a 15 per cent luminosity error at the flux limit, in agreement with the observed clusters.

The final expected number of clusters in cell $L_{\mathrm{X},i}$, z_j is then

$$N_{\mathrm{exp},ij} = \sum_k N_{\mathrm{mod},ik} P(L_{\mathrm{X},j}|L_{\mathrm{X},k}, \sigma_k)\, \mathrm{d}L_{\mathrm{X},j} \quad (18)$$

and the likelihood function is then

$$P(\boldsymbol{D}|\boldsymbol{\theta}) = \prod_{ij} P(N_{\mathrm{obs},ij}|N_{\mathrm{exp},ij}). \quad (19)$$

The probability distribution of the number of observed clusters N_{obs} is Poissonian, and can be simplified as before in our working limit of one or zero observed clusters per cell.

The posterior probability distribution was analysed using the *Laplace's Demon* package[1] for the *R* statistical computing environment (R Development Core Team 2012). An adaptive Metropolis Markov Chain Monte Carlo algorithm was used, and the resulting constraints on the model parameters are given in Table A1. The Schechter function shape parameters are all consistent with the results from the REFLEX data alone, indicating that the WARPS data do not provide much extra information to constrain those parameters. The confidence contours for the evolution parameters are plotted in Fig. 9. As expected, marginalizing over the uncertainties on the local XLF reduces the precision of the evolution measurements, though the presence of evolution [i.e. a difference from $A, B = (0, 0)$] is significant at more than 95 per cent. This is the first time that evolution in the cluster XLF has included this source of uncertainty. The best-fitting evolving Schechter function is compared with the low-redshift REFLEX Schechter function in Fig. 10.

The different evolution models are plotted in Fig. 11, which compares the number of clusters as a function of redshift predicted by the different model XLFs with that observed. The no-evolution REFLEX model clearly predicts more clusters than observed at

[1] http://www.bayesian-inference.com/software

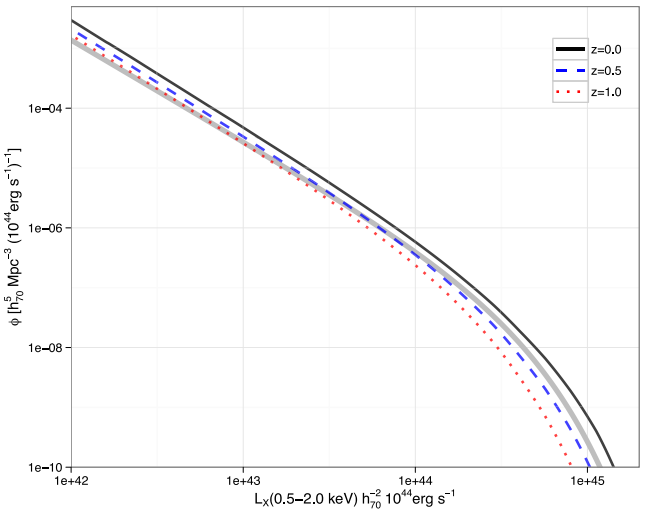

Figure 10. Schechter functions with best-fitting evolution parameters from the Bayesian analysis. The lines show the form of the Schechter function at redshifts 0, 0.5 and 1, and the grey line shows the REFLEX Schechter function.

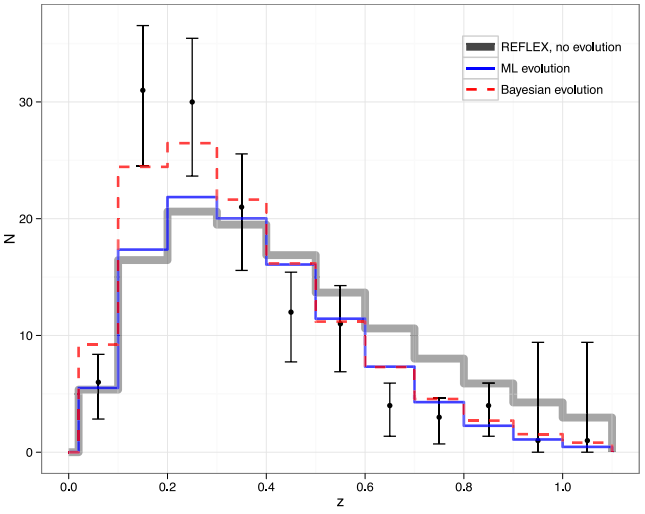

Figure 11. The observed redshift distribution of the WARPS clusters is compared to the distribution predicted by different models for the XLF. Both the ML and Bayesian fits are to the full sample ($z > 0.02$). The error bars on the observed counts are computed according to Gehrels (1986).

$z > 0.6$. There is some tension between the $z > 0.3$ ML fit and the Bayesian model, driven by the Bayesian model's accounting for the excess of WARPS clusters at $0.1 < z < 0.3$.

4.1.4 Cluster correlation function

We should also consider the likely contamination from any associated clusters that may lie on the line of sight to the sample cluster. Since the correlation function for clusters can be written as $\xi(r) = (r/r_0)^{-1.8}$, with the correlation length $r_0 \sim 20$ Mpc (e.g. Moscardini, Matarrese & Mo 2001; Basilakos & Plionis 2004), we can approximately integrate along the line of sight from, say, 2 Mpc (to represent the minimum possible separation) to ∼150 Mpc (where the correlation is negligible) to see that we expect close to twice as many clusters within this range as would be expected for an unclustered population. [We could alternatively integrate the two

Downloaded from http://mnras.oxfordjournals.org/ at NASA Goddard Space Flight Ctr on September 2, 2014

parameter $\xi(r_p, \pi)$ along $r_p = 0$ (e.g. Miller et al. 1999) to obtain essentially the same result.] Taking a column of length ± 150 Mpc and radius 1 Mpc centred on a given cluster (i.e. a volume $\sim 10^3$ Mpc^3 and a density of clusters around 10^{-5} Mpc^{-3}, appropriate for rather small clusters with only 10–20 bright early type galaxies (see e.g. Koester et al. 2007), we evidently expect only $\sim$1 per cent contamination by 'clustered clusters'. Reasonable changes to any of the values used here will only change this by a factor of a few. Indeed, if we are interested in contamination by large clusters (so that masses and fluxes are seriously affected), the number is around two orders of magnitude lower still.

4.2 Excess number density in low-z XLF

Figs 3, 5 and 11 show that the WARPS detects a significant excess of systems in the range $L_{\rm X(0.5–2.0\,keV)} = 1.0-2.0 \times 10^{43}$ erg s^{-1} and $0.1 < z < 0.3$ relative to the REFLEX Schechter function. These luminosities correspond to $\sim$2 keV systems, so are poor clusters or galaxy groups. Interestingly, a significant excess is seen at the same luminosity range in the 160SD low-z XLF. In determining this excess, we have been comparing observed number counts to the best-fitting model to the observed REFLEX XLF. It is worth considering whether an excess is present in the REFLEX data, but inspection of fig. 4 in Mullis et al. (2004) shows that the REFLEX data are close to the best-fitting Schechter function in this luminosity range (note their figure is for $H_0 = 50$ km s^{-1} Mpc^{-1}).

The best-fitting Bayesian XLF model predicts a significantly larger number of clusters at $z < 0.3$ than the REFLEX model, as shown in Fig. 12. This somewhat reduces the significance of the excess clusters in the bump at $L_{\rm X(0.5–2.0keV)} = 1.0-2.0 \times 10^{43}$ erg s^{-1}. Marginalized over the uncertainties on the model parameters, the Bayesian model predicts 16.5 ± 3.7 clusters, compared with the 28 observed. The probability of observing at least 28 clusters in this luminosity bump is 2 per cent. There is thus suggestive evidence that a real excess remains, and we now consider possible factors that could contribute to this.

Could the excess be simply a result of sample (cosmic) variance? The survey areas of WARPS and 160SD are much smaller than REFLEX, but the volumes surveyed are still significant. The clusters in the bump feature occupy the redshift range $0.1 < z < 0.3$ and the volume surveyed by WARPS in this redshift range is $\sim 10^7\, h_{70}^3$ Mpc^3. This volume is larger than the volumes in which sample variance is expected to be significant for galaxy surveys (Driver & Robotham 2010). For cluster surveys, Hu & Kravtsov (2003) provide analytical approximations to compute the relative contributions of Poisson noise and sample variance. Approximating the WARPS as a volume-limited survey with a mass threshold of $10^{14}\,{\rm M}_\odot$ at $z = 0.2$, the effects of Poisson noise and sample variance are approximately equal, with Poisson noise dominating at higher redshifts, and sample variance dominating at lower redshifts. This indicates that sample variance could be responsible for the excess cluster counts in the WARPS. However, it is more difficult for sample variance to explain the coincident, stronger, excess seen in the same part of the L,z plane in the 160 SD survey. Only 40 per cent of the WARPS fields and 35 per cent of the WARPS clusters are in common with 160SD. If the excess were due to sample variance, then the addition of extra, independent, fields should result in regression to the mean, not increased significance of the excess as observed. We thus conclude it is unlikely that the excess seen in both surveys is due to sample variance, and investigate other possibilities.

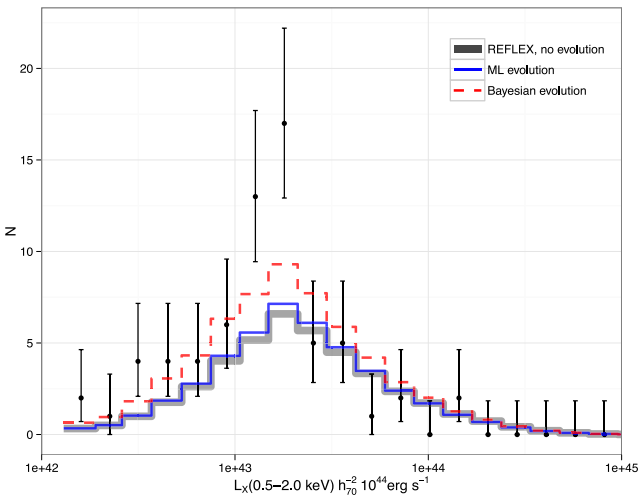

Figure 12. The observed luminosity distribution of the WARPS clusters at $z < 0.3$ is compared to the distribution predicted by different models for the XLF. The error bars on the observed counts are computed according to Gehrels (1986).

The three-dimensional distribution of the clusters in the luminosity and redshift range of the excess was examined, but there was no evidence for clustering in volume, so the excess is not caused by a superstructure of clusters. This is expected, since the selected fields are scattered across a large fraction of the sky.

A further possibility to explain the excess numbers is contamination in the detected flux from unresolved X-ray point sources, for example low-luminosity active galactic nuclei (AGN). Such contamination was removed where possible, but not all contaminating sources are resolved in the *ROSAT* PSPC images. Hence, some residual contamination is expected, enhancing the estimated cluster luminosities. Detailed modelling of the AGN population is beyond the scope of this paper, but this contamination would differ from the scatter models discussed above, as the effect is purely additive. Some mass or redshift dependence of the AGN contamination may be required to manifest the localized excess of clusters in the $L_{\rm X}$,z plane.

Finally, we consider if selection bias may be responsible for the excess clusters seen in this region of the $L_{\rm X}$,z plane. This is plausible, given that the excess is close to the flux limit in the region of the $L_{\rm X}$,z plane where the WARPS is most sensitive (see Fig. 1). Eddington bias enhances cluster number counts when scatter is present in the luminosities of the population. The slope of the XLF means that for a given flux limit, there are more clusters below the flux limit that may scatter into the sample than above the flux limit that may scatter out of the sample. There are two sources of scatter that may be important: statistical scatter due to the counting statistics on the $L_{\rm X}$ measurement, and intrinsic scatter in the cluster population. Our Bayesian analysis allows us to investigate each of these sources of scatter in turn, by modifying the model for the population scatter in equation (18).

Note that if the population scatter is constant with $L_{\rm X}$ and z, then a bias is present at all redshifts and luminosities, and increases towards higher luminosities due to the steepening of the XLF, so would not produce a localized excess in the L_x,z plane. However, the statistical scatter decreases with increasing $L_{\rm X}$, as $\sim \sqrt{N}$ errors decrease above the flux limit, and increase below it. This gives rise to a bias that is strongest near the flux limit, with counting statistics allowing clusters nominally too faint for the sample to appear above the flux limit, so could plausibly contribute to the observed excess. However, the typical measurement error on luminosities close to the

Downloaded from http://mnras.oxfordjournals.org/ at NASA Goddard Space Flight Ctr on September 2, 2014

flux limit is ≈15 per cent, and even modelling the increasing flux scatter below the flux limit, the bias due to this source of scatter was found to contribute <1 additional cluster in the regions of the excess, compared to models with no scatter. We note, however, that our model for the scaling of the statistical scatter with flux is simplistic – the measurement errors also depend on the exposure time and background level in the source field. Modelling this for clusters below the flux limit would require extensive simulations and is beyond the scope of this work.

The intrinsic scatter in luminosity of the cluster population is known to be significant, and if this varies with mass or redshift, it could result in a bias that contributed to a localized excess in number counts. The variation of cluster scatter with mass is not well measured, but there is evidence that the intrinsic luminosity scatter decreases above $z \approx 0.4$ (Maughan 2007), albeit measured in a heterogeneous sample. We test the effect that evolving scatter could have on the measured XLF by replacing the scatter model in equation (18) with a lognormal distribution, with a standard deviation of 50 per cent at $z < 0.45$, decreasing smoothly to 20 per cent at $z > 0.55$ (Maughan 2007). The effect of this evolving scatter is to increase the number of $z < 0.3$ clusters predicted by the Bayesian model by ≈10 per cent, but this still leaves a significant excess of observed clusters at around $L_{\mathrm{X(0.5–2.0\,keV)}} = 1.0-2.0 \times 10^{43}\,\mathrm{erg\,s^{-1}}$.

Similarly, introducing an ad hoc model of intrinsic scatter which decreases from 90 per cent to 20 per cent at $L_{\mathrm{X(0.5–2.0\,keV)}} = 2.5 \times 10^{43}\,\mathrm{erg\,s^{-1}}$ (designed to maximize the Eddington bias effect) only serves to increase the model prediction by 2.5 clusters in the bins contributing to the excess. When compared to the REFLEX XLF, the observed excess of WARPS clusters remains highly significant in the face of all bias contributions.

A luminosity of $2 \times 10^{43}\,\mathrm{erg\,s^{-1}}$ corresponds to a mass of $M_{200} \simeq 10^{14}\,\mathrm{M_\odot}$, at the borderline between groups and clusters. It is possible that some features of the cluster population in this region of the L_X,z plane enhance their detectability, by e.g. enhancing their surface brightness. This could result from, for instance, an enhanced AGN or cool-core population, but the effects would need to be relatively localized in L_X and z. With the present data it is not possible to investigate this further, but with the arrival of new deep cluster surveys such as XXL or XCS, it should be possible to verify these results and extend the investigation.

4.3 Sensitivity to high-redshift cool-core clusters

Since the detection of clusters in X-ray surveys is driven by their surface brightness, the presence or absence of centrally peaked emission associated with a cool core may have a strong impact on the detection of a given cluster. There is some debate in the literature as to whether there are significant numbers of cool-core clusters in the high-z ($z > 0.5$) Universe. Both Vikhlinin et al. (2007) and Santos et al. (2010) find a lack of high-z cool-core clusters in the distant 400SD sample, but Santos et al. (2010) find evidence for moderate cool cores in high-z clusters detected in the WARPS and RDCS. They argue that the 400SD (and by extension 160SD) may have discarded high-z cool-core clusters as being unresolved, but note that this does not imply incompleteness in the 400SD provided the surface brightness dependence was modelled into the selection function.

The excellent agreement of the evolution in the XLF seen in the WARPS and 160SD at $z > 0.3$ despite their very different cluster detection algorithms implies that this is indeed the case, and that there are no significant problems with the selection function of either survey. We also note that the comparisons of clusters detected or missed by WARPS and 160SD in 157 common fields revealed no significant discrepancies, with differences being explained by the differing selection criteria (Horner et al. 2008).

5 CONCLUSIONS

We measured the evolution of the XLF out to $z \sim 1$ from the combined WARPS-I and WARPS-II surveys, finding significant evidence for negative evolution, in the sense of a reduction in the number density of massive luminous clusters with redshift. This is confirmed by comparing expected and observed numbers, and more convincingly by the ML analysis. This is consistent with previous measurements of the evolution of the XLF, and the expectations of hierarchical structure formation in a ΛCDM universe.

We investigate the sensitivity of these results to various sources of systematic uncertainty affecting the WARPS XLF and selection function. The results are not significantly affected by the modelling of the core radii of the clusters, the assumed upper redshift limit of the survey, or the technique used for estimating detection volumes for the clusters. The assumed value of $z_{\mathrm{max}} = 1.1$ is fairly conservative, as there is a cluster detected at $z = 1.05$ and many of the clusters would be detectable in X-rays to significantly higher redshift. Thus the true evolution could be somewhat stronger than we measure.

For the first time, we fully incorporate the uncertainties on the low-redshift XLF into a Bayesian analysis of the evolution, and find that while the precision of the measurements is reduced, evolution is still significant at the 95 per cent level.

The good agreement of the measured evolution in the WARPS, 160SD and other surveys suggests that the result is not sensitive to the details of the cluster detection and follow-up strategy, and that the selection functions of both surveys are accurately modelled, including the effects of cool cores on the detectability of clusters.

We identified a significant excess of ∼2 keV systems at $z < 0.3$ observed in both the WARPS and 160SD surveys relative to the REFLEX XLF. A Bayesian fit to the WARPS data, which uses the REFLEX measurements as priors, yields a model with slightly higher ϕ^* and α values than REFLEX, and reduces the excess. However, even with this model, and with including possible contributions from Eddington bias, the excess remains significant. The cause of the excess is not clear at present, although its presence in both the WARPS and 160SD argue against it being a result of a mis-calibrated selection function. New, more sensitive measurements of the XLF with surveys like *XXL* (Pierre et al. 2011) and *XCS* (Mehrtens et al. 2011) will provide better statistics for this part of the L_X,z plane, providing a means to address this question further.

ACKNOWLEDGEMENTS

We thank Chris Collins and Andy Young for useful discussions. LK acknowledges support from the European Research Council under the EC FP7 grant number 240185. This research has made use of data obtained from the High Energy Astrophysics Science Archive Research Center (HEASARC), provided by NASA's Goddard Space Flight Center.

REFERENCES

Avni Y., Bahcall J. N., 1980, ApJ, 235, 694
Barkhouse W. A. et al., 2006, ApJ, 645, 955
Basilakos S., Plionis M., 2004, MNRAS, 349, 882

Downloaded from http://mnras.oxfordjournals.org/ at NASA Goddard Space Flight Ctr on September 2, 2014

Böhringer H. et al., 2001, A&A, 369, 826
Böhringer H. et al., 2002, ApJ, 566, 93
Borgani S., Rosati P., Tozzi P., Norman C., 1999, ApJ, 517, 40
Burenin R. A., Vikhlinin A., Hornstrup A., Ebeling H., Quintana H, Mescheryakov A., 2007, ApJS, 172, 561
Burke D. J., Collins C. A., Sharples R. M., Romer A. K., Nichol R. C., 2003, MNRAS, 341, 1093
Castander F. J. et al., 1995, Nat, 377, 39
de Grandi S. et al., 1999, ApJ, 514, 148
Driver S. P., Robotham A. S. G., 2010, MNRAS, 407, 2131
Ebeling H., Wiedenmann G., 1993, Phys. Rev. E, 47, 704
Ebeling H., Edge A. C., Bohringer H., Allen S. W., Crawford C. S., Fabian A. C., Voges W., Huchra J. P., 1998, MNRAS, 301, 881
Ebeling H., Edge A. C., Allen S. W., Crawford C. S., Fabian A. C., Huchra J. P., 2000, MNRAS, 318, 333
Ebeling H., Edge A. C., Henry J. P., 2001, ApJ, 553, 668
Edge A. C., Stewart G. C., Fabian A. C., Arnaud K. A., 1990, MNRAS, 245, 559
Ellis S. C., Jones L. R., 2002, MNRAS, 330, 631
Fassbender R. et al., 2011, New J. Phys., 13, 125014
Gehrels N., 1986, ApJ, 303, 336
Gioia I. M., Henry J. P., Maccacaro T., Morris S. L., Stocke J. T., Wolter A., 1990a, ApJ, 356, L35
Gioia I. M., Maccacaro T., Schild R. E., Wolter A., Stocke J. T., Morris S. L., Henry J. P., 1990b, ApJS, 72, 567
Gioia I. M., Henry J. P., Mullis C. R., Voges W., Briel U. G., Böhringer H., Huchra J. P., 2001, ApJ, 553, L105
Henry J. P., Gioia I. M., Maccacaro T., Morris S. L., Stocke J. T., Wolter A., 1992, ApJ, 386, 408
Henry J. P., Gioia I. M., Mullis C. R., Voges W., Briel U. G., Böhringer H., Huchra J. P., 2001, ApJ, 553, L109
Horner D. J., Perlman E. S., Ebeling H., Jones L. R., Scharf C. A., Wegner G., Malkan M., Maughan B., 2008, ApJS, 176, 374
Hu W., Kravtsov A. V., 2003, ApJ, 584, 702
Jones L. R., Scharf C., Ebeling H., Perlman E., Wegner G., Malkan M., Horner D., 1998, ApJ, 495, 100
Jones L. R. et al., 2000, in Plionis M., Georgantopoulos I., eds, Large Scale Structure in the X-ray Universe. Atlantisciences, Paris, France, p. 35
Kaiser N., 1986, MNRAS, 222, 323
Koester B. P. et al., 2007, ApJ, 660, 239
Linder E. V., 2005, Phys. Rev. D., 72, 043529
Mantz A., Allen S. W., Ebeling H., Rapetti D., 2008, MNRAS, 387, 1179
Mantz A., Allen S. W., Rapetti D., Ebeling H., 2010, MNRAS, 406, 1759
Markevitch M., 1998, ApJ, 504, 27
Marshall H. L., Tananbaum H., Avni Y., Zamorani G., 1983, ApJ, 269, 35
Mason K. O. et al., 2000, MNRAS, 311, 456
Maughan B. J., 2007, ApJ, 668, 772
Maughan B. J., Jones C., Forman W., Van Speybroeck L., 2008, ApJS, 174, 117
Mehrtens N. et al., 2011, MNRAS, 423, 1024
Miller C. J., Batuski D. J., Slinglend K. A., Hill J. M., 1999, ApJ, 523, 492
Moretti A. et al., 2001, in Riccardo G., Salvatore S., Luigi S., eds, ASP Conf. Ser. Vol. 234, X-ray Astronomy 2000, Astron. Soc. Pac., San Francisco, p. 393
Moscardini L., Matarrese S., Mo H. J., 2001, MNRAS, 327, 422
Mullis C. R. et al., 2003, ApJ, 594, 154
Mullis C. R. et al., 2004, ApJ, 607, 175
Page M. J., Carrera F. J., 2000, MNRAS, 311, 433
Panzera M. R., Campana S., Covino S., Lazzati D., Mignani R. P., Moretti A., Tagliaferri G., 2003, A&A, 399, 351
Perlman E. S., Horner D. J., Jones L. R., Scharf C. A., Ebeling H., Wegner G., Malkan M., 2002, ApJS, 140, 265
Pierre M., Pacaud F., Juin J. B., Melin J. B., Valageas P., Clerc N., Corasaniti P. S., 2011, MNRAS, 414, 1732
R Development Core Team, 2012, R: A Language and Environment for Statistical Computing. R Foundation for Statistical Computing, Vienna, Austria
Romer A. K. et al., 2000, ApJS, 126, 209
Rosati P., Della Ceca R., Burg R., Norman C., Giacconi R., 1995, ApJ, 445, L11
Rosati P., Della Ceca R., Norman C., Giacconi R., 1998, ApJ, 492, L21
Santos J. S., Tozzi P., Rosati P., Böhringer H., 2010, A&A, 521, A64
Scharf C. A., Jones L. R., Ebeling H., Perlman E., Malkan M., Wegner G., 1997, ApJ, 477, 79
Schechter P., 1976, ApJ, 203, 297
Schmidt M., 1968, ApJ, 151, 393
Schuecker P., Böhringer H., Collins C. A., Guzzo L., 2003, A&A, 398, 867
Smith R. K., Brickhouse N. S., Liedahl D. A., Raymond J. C., 2001, ApJ, 556, L91
Vikhlinin A., McNamara B. R., Forman W., Jones C., Quintana H., Hornstrup A., 1998, ApJ, 502, 558
Vikhlinin A., Burenin R., Forman W. R., Jones C., Hornstrup A., Murray S. S., Quintana H., 2007, Heating versus Cooling in Galaxies and Clusters of Galaxies. Springer-Verlag, Berlin, p. 48
Vikhlinin A. et al., 2009, ApJ, 692, 1060

APPENDIX A: XLF TABLES

For future reference we present tables of the binned XLF. Per bin we also quote the number of observed clusters, their median redshift $\tilde{z}$ and their average X-ray luminosity $\overline{L}_{\rm X}$ (see Table A1).

Downloaded from http://mnras.oxfordjournals.org/ at NASA Goddard Space Flight Ctr on September 2, 2014

Table A1. The XLF for the local, the intermediate-redshift and high-redshift universe as measured by WARPS. Also shown are the observed number of clusters $N_{\rm obs}$, their median redshift $\tilde{z}$, and their average luminosity $\overline{L}_{\rm X}$.

$L_{\rm X,centre}$ (0.5–2.0 keV) [h_{70}^{-2} 10^{44} erg s^{-1}]	ϕ [h_{70}^{5} Mpc^{-3} (10^{44} erg s^{-1})$^{-1}$]	$\phi^{+1\sigma}$ [$h_{70}^{5}\,y$ Mpc^{-3} (10^{44} erg s^{-1})$^{-1}$]	$\phi^{-1\sigma}$ [h_{70}^{5} Mpc^{-3} (10^{44} erg s^{-1})$^{-1}$]	$N_{\rm obs}$	$\tilde{z}$	$\overline{L}_{\rm X}$ (0.5–2.0 keV) [h_{70}^{-2} 10^{44} erg s^{-1}]
$0.02 < z < 0.3$						
0.011	2.26×10^{-3}	7.46×10^{-2}	3.91×10^{-4}	1	0.051	0.010
0.016	1.14×10^{-3}	2.64×10^{-2}	4.04×10^{-4}	2	0.063	0.015
0.022	2.33×10^{-4}	7.69×10^{-4}	4.03×10^{-3}	1	0.107	0.025
0.031	3.46×10^{-4}	6.20×10^{-4}	1.80×10^{-4}	4	0.125	0.032
0.044	1.33×10^{-4}	2.38×10^{-4}	6.94×10^{-5}	4	0.119	0.043
0.063	5.72×10^{-5}	1.02×10^{-4}	2.98×10^{-5}	4	0.151	0.060
0.089	3.53×10^{-5}	5.64×10^{-5}	2.13×10^{-5}	6	0.150	0.090
0.125	3.68×10^{-5}	5.01×10^{-5}	2.67×10^{-5}	13	0.193	0.125
0.177	2.25×10^{-5}	2.94×10^{-5}	1.71×10^{-5}	17	0.226	0.174
0.251	4.85×10^{-6}	8.13×10^{-6}	2.75×10^{-6}	5	0.252	0.233
0.355	3.24×10^{-6}	5.43×10^{-6}	1.84×10^{-6}	5	0.240	0.352
0.502	4.82×10^{-7}	1.59×10^{-6}	8.34×10^{-8}	1	0.242	0.457
0.710	6.51×10^{-7}	1.51×10^{-6}	2.30×10^{-7}	2	0.244	0.741
1.004	0	8.98×10^{-7}	0	0	*n.a.*	*n.a.*
1.420	3.25×10^{-7}	7.54×10^{-7}	1.15×10^{-7}	2	0.292	1.351
$0.3 < z < 0.6$						
0.177	2.07×10^{-5}	4.79×10^{-5}	7.31×10^{-6}	2	0.304	0.196
0.251	4.23×10^{-6}	8.35×10^{-6}	1.93×10^{-6}	3	0.315	0.259
0.355	2.78×10^{-6}	4.28×10^{-6}	1.75×10^{-6}	7	0.370	0.373
0.502	1.31×10^{-6}	1.96×10^{-6}	8.56×10^{-7}	8	0.378	0.507
0.710	6.68×10^{-7}	9.53×10^{-7}	4.60×10^{-7}	10	0.461	0.707
1.004	3.54×10^{-7}	5.29×10^{-7}	2.32×10^{-7}	8	0.502	1.006
1.420	8.94×10^{-8}	1.76×10^{-7}	4.08×10^{-8}	3	0.500	1.455
2.008	4.42×10^{-8}	1.02×10^{-7}	1.56×10^{-8}	2	0.561	1.909
2.840	1.56×10^{-8}	5.16×10^{-8}	2.71×10^{-9}	1	0.517	2.730
$0.6 < z < 1.1$						
1.004	1.01×10^{-7}	3.33×10^{-7}	1.74×10^{-8}	1	0.679	1.110
1.420	7.34×10^{-8}	1.45×10^{-7}	3.35×10^{-8}	3	0.722	1.421
2.008	4.87×10^{-8}	8.17×10^{-8}	2.77×10^{-8}	5	0.832	2.114
2.840	0	2.51×10^{-8}	0	0	*n.a.*	*n.a.*
4.016	5.88×10^{-9}	1.36×10^{-8}	2.08×10^{-9}	2	0.820	4.164
5.680	2.08×10^{-9}	6.86×10^{-9}	3.60×10^{-10}	1	0.833	6.655
8.032	1.47×10^{-9}	4.85×10^{-9}	2.54×10^{-10}	1	0.892	9.271

This paper has been typeset from a TEX/LATEX file prepared by the author.

Downloaded from http://mnras.oxfordjournals.org/ at NASA Goddard Space Flight Ctr on September 2, 2014